Colloids and Surfaces B: Biointerfaces 233 (2024) 113641

Contents lists available at ScienceDirect

Colloids and Surfaces B: Biointerfaces

journal homepage: www.elsevier.com/locate/colsurfb

Mechanically robust, transparent, and UV-shielding composite of Na-Alginate and maleic acid-functionalized boron nitride nanosheets with improved antioxidant property

Timo Elo [a], Vijay Singh Parihar [b], Abhijit Bera [c], Farzin Javanshour [d], Minna Kellomäki [b], Rama Layek [a,*]

[a] LUT University, School of Engineering Science, Department of Separation Science, Mukkulankatu 19, 15210 Lahti, Finland
[b] Biomaterials and Tissue Engineering Group, BioMediTech, Faculty of Medicine and Health Technology, Tampere University, Finland
[c] Midnapore College (Autonomous), Raja Bazar Main Rd., 721101, Midnapore, India
[d] Unit of Materials Science and Environmental Engineering, Tampere University, Tampere, Finland

ARTICLE INFO

Keywords:
Maleic Acid functionalized Boron nitride nanosheet
Sodium Alginate
Biopolymer composite
Mechanical property
UV-shielding property
Antioxidant property

ABSTRACT

Maleic acid functionalized boron nitride nanosheets (BNNS-MA)/Na-Alginate composite with enhanced mechanical, UV-shielding and antioxidation properties have been fabricated for the first time by solvent evaporation from a homogeneous aqueous dispersion of BNNS-MA/Na-Alginate composite solution. The composite fabrication was driven by homogenous nano-integrations and chemistry of compatibilization of BNNS-MA with Na-Alginate through H-bonding interactions between -COOH functional group of BNNS-MA and -OH, -COONa groups of Na-Alginate. The BNNS-MA/Na-Alginate composites show significant enhancement of mechanical, UV-blocking and antioxidant properties compared to the Na-Alginate. Integrating only 1 wt% BNNS-MA improved the UV-blocking, tensile strength, and antioxidant properties of Na-Alginate film by 99.1%, 73% and 60.3%, respectively. Overall, our findings of BNNS-MA integrated Na-Alginate composite films with improved physical, mechanical, UV shielding, and antioxidant functionalities is very promising to open new insight in the field of transparent UV-protected biopolymer film for consumer products, packaging, cosmetics, and engineering applications.

1. Introduction

At current scenario, over 300 million tons of plastic are produced worldwide each year and 50% of that is used for packaging purposes [1]. Generally, petroleum oil-derived synthetic polymeric films such as polyethylene, polypropylene, polyvinyl chloride, polystyrene, polyethylene terephthalate and their nanocomposites are typically used for packaging applications due to the ease of availability, lightweight, excellent physical, and mechanical properties [2]. These petroleum resource derived polymers do not degrade in the environment after use and cause environmental pollution. Hence, the demand for renewable biopolymers for environmentally friendly and sustainable packaging film is consistently growing to replace petroleum oil-derived polymers for packaging applications [3,4].

Among the various biopolymer varieties, Na-Alginate is a very important biobased and biodegradable biopolymer that is easily acquired from brown algae and exhibits very good film-forming abilities [5]. Due to their outstanding biocompatibility and biodegradability, Na-Alginate based biopolymer films are gaining remarkable attention as an alternative to petroleum-derived polymers for consumer products, packaging, cosmetics, and engineering applications [6]. Hence, it is considered as an appropriate biopolymer for environmentally friendly consumer products, packaging, and engineering products design [7]. The efficient biopolymeric materials should have excellent UV-shielding property along with remarkable mechanical, antioxidant, and radical scavenging properties to enhance the shelf life of perishable goods such as medicine, health, beauty, cosmetics, and foods; consumers and engineering optical products [8,9]. However, the poor mechanical property and inadequate UV-shielding, antioxidant and radical scavenging properties limit the application of Na-Alginate films in eco-friendly consumer products, engineering product design and packaging as an alternative of petroleum resource derived polymer film. In recent

* Corresponding author.
E-mail address: rama.layek@lut.fi (R. Layek).

https://doi.org/10.1016/j.colsurfb.2023.113641
Received 21 August 2023; Received in revised form 30 October 2023; Accepted 7 November 2023
Available online 8 November 2023

studies, the judicial integration of various types of multifunctional additives such as carbon nanotube, graphene, carbon black, lignin, and tannin into polymer and biopolymer matrixes have been explored to improve the mechanical and UV-shielding, antioxidation and radical scavenging functionalities of the polymer and biopolymer composites [10,11].

Boron nitride nanosheet (BNNS) is a ceramic material with a wide band gap composed of alternating boron and nitrogen atoms. The B and N atoms are arranged in a hexagonal pattern with a fused conjugated aromatic ring structure analogous to graphene. Therefore, BNNS and graphene have comparable properties in terms of mechanical strength, excellent UV-shielding and antioxidant properties, and outstanding thermal conductivity [12]. Among the various types of physicochemical functionalities, one of the most promising properties of BNNS is an enhancement of UV-light shielding functionalities of the polymer composites without degradation. In addition, BNNS shows excellent biocompatibility [13] and antioxidant properties [14]. Hence, judicial integration of the multifunctional BNNS additives into Na-Alginate biopolymer films can be a promising method to create a synergy between enhancing the mechanical performance, UV-shielding, antioxidation as well as radical scavenging functionalities.

BNNS can be produced either by bottom-up methods, such as chemical vapor deposition (CVD) [15], or top-down approaches, including micro-mechanical cleavage (MMC) and exfoliation of bulk BN. Although, CVD and MMC produce high-quality BNNS, the production yield is very low, which limits application of CVD and MMC in the field of BNNS-based polymer nanocomposites. On the other hand, exfoliation of BN produces relatively defective BNNS compared to CVD and MMC methods, but in the scalable quantities suitable for polymer composite applications [16]. However, similarly to graphene, one of the most significant problems with using BNNS as a nanofiller is related to its processability. This is due to the high cohesive van der Waals energy between BNNS layers, BNNS precipitating from most common solvents and being incompatible with both hydrophilic and hydrophobic polymers. Therefore, the functionalization of BNNS with suitable functional groups is crucial to enhance for its compatibility with polymers and to fabricate high-performance polymer composite with improved functionalities [17–23]. Nevertheless, the substantial research efforts devoted in functionalizing BNNS for fabrication of high-performance polymer composite to the best of our knowledge, there has not been any report on the effect of BNNS integrated sustainable biopolymer composites film with UV-shielding, antioxidant, and radical scavenging properties in a single biocomposite system for biobased sustainable packaging and cosmetics application.

Very recently, we have synthesized a scalable quantity of BNNS functionalized maleic acid (BNNS-MA) via Diels Alder reaction that is reflected as a promising nanofiller for high-performance polymer composite with hydrophilic polymers [24]. In this paper, we report a novel alternative transparent biocomposite film of sodium alginate via judicially integrating BNNS-MA that shows significant enhancement of physical, mechanical, UV-blocking, and anti-oxidation properties for the first time. Na-Alginate is a hydrophilic biopolymer with several carboxylate and hydroxyl functional groups on its surface. BNNS-MA is hydrophilic in nature due to the presence of numerous carboxyl functional groups, which easily interact with carboxylate and hydroxyl functional groups of Na-Alginate and produce a homogeneous biocomposite with excellent functionalities. The obtained BNNS-MA/Na-Alginate nanocomposite films exhibits significant improvement of mechanical strength, and UV-blocking properties with integration of 1 wt% of BNNS-MA. In addition, the nanocomposite film shows better antioxidation as well as radical scavenging functionality compared to pure Na-Alginate film. The enhanced physical, mechanical, UV-blocking, and anti-oxidation properties of the BNNS-MA/Na-Alginate biocomposite films could be applied to a wide range of biobased consumer, cosmetics, and engineering products, as well as packaging film.

2. Experimental section

2.1. Materials and Methods

Sodium alginate (Alginic acid sodium salt from brown algae, Sigma-Aldrich), boron nitride (size ~1 μm, Sigma-Aldrich), and maleic Anhydride (≥98%, VWR international Oy) were used as received. Distilled water (DI-water) was used for this study. PTFE membrane with pore size of 0.2 μm was used as received from sigma-Aldrich.

2.1.1. Synthesis of BNNS-MA

The BNNS-MA was synthesized by Diels-Alder reaction following our previously reported procedure [24]. In brief, first, BN and maleic Anhydride were blended in 1:5 ratio mechanically. Then blended mixture was kept in a sealed vessel of inert nitrogen atmosphere and treated at 180 ℃ for 4 h. After that reaction mixture was cooled down to room temperature and transferred into a beaker by adding 100 mL of DI-water. Final volume of the reaction mixture was adjusted approximately 500 mL by addition of another 400 mL of DI-water with the reaction mixture. Then, the reaction mixture was sonicated for 30 min to produce a homogeneous aqueous dispersion of white color BNNS-MA hybrids. Finally, BNNS-MA was collected by removing unreacted chemicals from aqueous dispersion of BNNS-MA hybrids via vacuum filtration through PTFE (Polytetrafluoroethylene) membrane and simultaneous repeated washing with DI-water followed by drying in a vacuum oven at 50 ^{0}C.

2.1.2. Preparation of Na-Alginate/BNNS-MA composite film

The homogeneous aqueous solution of Na-Alginate was prepared by dissolving 1 g of Na-Alginate in 15 mL DI-water in three different vessels. Then, desired amounts of BNNS-MA were dispersed in 5 mL of water by ultrasonication and blended with aqueous solution of Na-Alginate by mechanical stirring to produced 0.25, 0.5 and 1 wt% of BNNS-MA composite solution with respect to Na-Alginate. Finally, these composite solutions were poured into glass petri dishes, and evaporated at room temperature to obtain free standing Na-Alginate/BNNS-MA composites film. Then, these obtained Na-Alginate/BNNS-MA composites film were kept for additional 24 h in a fume cupboard under air flow to remove any remaining water in the composite film if any. The composite films are designated as BNNS-MA 0.25, BNNS-MA 0.5, and BNNS-MA 1, where the numbers after BNNS-MA represent the weight percentage of BNNS-MA with respect to Na-Alginate. To provide a basis for comparison, pure boron nitride was subjected to the same processing conditions employed in the preparation of BNNS-MA, except without the use of any maleic anhydride. Subsequently, a composite film containing 1 wt% of this processed boron nitride sheets (BNS) was prepared by incorporating it into a sodium alginate matrix.

3. Characterization

Samples for atomic force microscopy (AFM) study was performed via casting a drop of an aqueous dispersion of BNNS-MA (0.01% w/v) on a HOPG surface, followed by evaporating the solvent at room temperature. Then, AFM studies of GO over a HOPG surface were carried out in noncontact mode using a tip resonance frequency of 250 KHz with SEM Zeiss ULTRA Plus instrument. FTIR spectroscopy measurements of BNNS-MA/Na-Alginate composites were carried out in ATR mode at resolution of 4 cm^{-1} in 4000–400 cm^{-1} range with Bruker Alpha-P instrument using diamond tip. Cross-sectional FESEM study of the cryo-fractured BNNS-MA/Na-Alginate composites was performed using JEOL JSM-7900 F instrument. Wide angle X-ray scattering (WAXS) of BNNS-MA/Na-Alginate composites were performed via fixing sample on sample holder and scanning it in 2θ range of 5° to 80 ° at a rate of increment of 0.015 with step time of 0.3 s using Bruker AXS D8 ADVANCE instrument. A Cu tube as a radiation source was used and the operating voltage and current of the instrument were 40 kV and 40 mA,

respectively. TGA study of BN, BNNS-MA and BNNS-MA/Na-Alginate composites were performed under nitrogen atmosphere at heating rate of 10 ℃/min using TGA-Q-500 instrument. The UV–vis spectroscopy of Na-Alginate, BNS/Na-Alginate and BNNS-MA/Na-Alginate composite film were recorded in transmittance mode by passing UV–vis light through a specimen using UV-6300PC Double Beam Spectrometer. Mechanical property of the Na-Alginate, BNS/Na-Alginate and BNNS-MA/Na-Alginate composite with specimen size 16 mm × 4 mm x 0.10 mm were studied using Instron 5967 instrument at a strain rate of 1 mm/ min at 30 ℃. The antioxidant and radical scavenging study was done by treating the BNS 1 and BNNS-MA 1 with 2,2-diphenyl-1-picryl-hydrazyl (DPPH) solution and measuring absorbance difference of DPPH solution between control and test samples in the UV–vis spectra at wavelength 517 nm with UV-3600 Plus spectrometer.

4. Results and discussion

4.1. Functionalization of BNNS with Maleic anhydride (BNNS-MA) and its Nanocomposites with Na-Alginate

Due to the high cohesive van der Waals energy between the BN layers, BN powder does not uniformly disperse in aqueous medium. it is reported in previous literatures that directly exfoliating bulk h-BN through only sonication in a liquid medium [25] is very challenging task. This method often necessitates prolonged sonication and harsh conditions to achieve exfoliation, yielding only a fraction of BN sheets reduced to a few layers. It is noteworthy that h-BN shares an isoelectronic structure with graphite, exhibiting conjugated double bonds (B═N) analogous to C═C in graphite/graphene [26]. Previous studies have demonstrated that graphite can undergo a Diels-Alder reaction with maleic anhydride, resulting in the scalable production of maleic anhydride-functionalized graphene sheets [27]. Similarly, h-BN can react with maleic anhydride in a similar manner to graphite, involving a Diels-Alder reaction to initially produce maleic anhydride-functionalized h-BN sheets. The unsaturated units of maleic anhydride form covalent bonds through cycloaddition reactions with boron nitride sheets, a process similar to reactions observed in other 2-D materials [27–29]. The cyclic rings formed as a result of these cycloaddition reactions can interact covalently with the aromatic sheet structure of BN, thereby reducing van der Waals (VDW) interactions among the layers of BN. In aqueous medium, maleic anhydride unit of maleic anhydride functionalized BN is converted into maleic acid (MA) unit. Hence, the presence of -COOH groups in MA unit of maleic acid functionalized boron nitride sheet contributes to its strong affinity for polar solvents such as water. This affinity assists in reducing VDW interactions among the layers of BN in an aqueous medium and consequently, short period (30 min) of ultrasonic treatment in an aqueous medium can induce the delamination and large-scale exfoliation of BNNS-MA. Diels-Alder reaction of BN with maleic anhydride, followed by sonication and repeated washing with water produces BNNS-MA. The details chemistry of functionalization and characterization of BNNS-MA was shown in our previous study [24]. To investigate the morphology and exfoliation of BNNS-MA, AFM images and corresponding height profile of BNNS-MA are presented in Fig. 1a-c. Fig. 1a-b shows AFM image after casting a drop of dilute aqueous dispersion of BNNS-MA on HOPG surface, which demonstrates that BNNS-MA produces an exfoliated sheet like structure in dilute aqueous solution. The height profile of the BNNS-MA obtained from the AFM image shown in Fig. 1c, and it shows that majority of the BNNS-MA sheets exhibit thickness in between 0.60.60 nm and 1.3 nm. There are also few sheets with a thickness of 0.40 nm and thickness higher than 1.3 nm that were observed. It is stated in prior art literature that average thickness of monolayer BNNS is experimentally 0.32 nm and theoretically 0.34 nm [30,31]. Hence, our BNNS-MA typically consists of few single sheets, while majority of sheets exhibit 2-4 layers along with few multilayer sheets in dilute aqueous solution [30,31].

4.2. BNNS-MA integrated Na-Alginate composite

Na-Alginate is a very important biopolymer composed of a linear chain of alternating blocks of β-D-Mannuronic acid (M) and α-L-guluronic acid (G) (1−4) linked residues, that are in heteropolymeric (MG) and/or homopolymeric (M or G) arrangements [7,32]. It shows excellent solubility in water due to presence of several oxygen containing hydrophilic functional groups (-OH and -COO^- Na^+). BNNS-MA displays very good dispersion in aqueous medium due to the presence of -COOH group on its surface. The mixing of aqueous dispersion of BNNS-MA with aqueous solution of Na-Alginate produces stable homogenous aqueous dispersion and this is due to H-bonding interaction between the oxygen containing functional group of BNNS-MA and Na-Alginate. The evaporation of water from aqueous solution of pure Na-Alginate and BNNS-MA/Na-Alginate hybrids at room temperature produced good quality films with uniform thickness. The pure Na-Alginate produce very transparent film whereas the BNNS-MA/Na-Alginate composite film shows slight white color with significant transparency. The structure-property co-relationship of the obtained BNNS-MA/Na-Alginate composites were investigated by characterizing the samples using WAXS, FTIR, TGA, UTM, studying the morphology of composites via FESEM analysis and investigating the UV-shielding and antioxidant property using UV–vis spectroscopy.

4.3. WAXS study

To investigate the structure of BNNS-MA/Na-Alginate composites WAXS studies of BNNS-MA, Na-Alginate and BNNS-MA/Na-Alginate composites were carried out and are presented in Fig. 2. It is clear

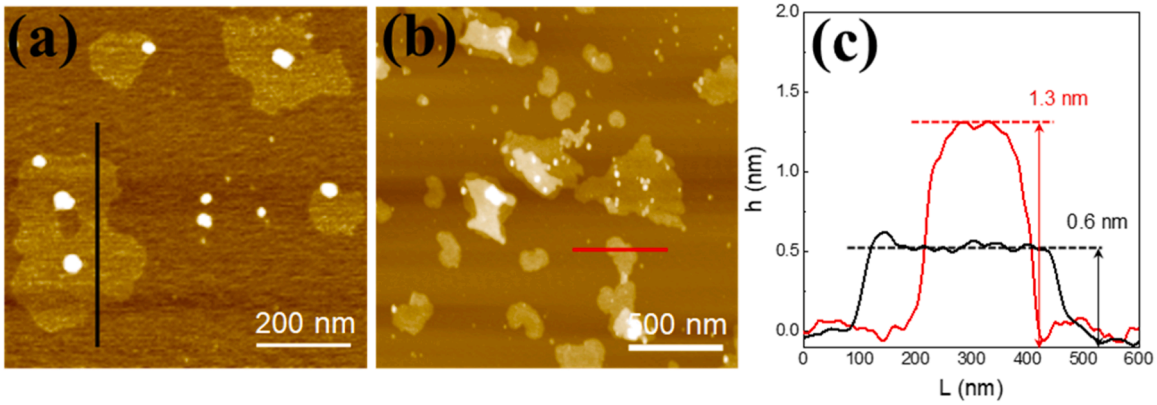

Fig. 1. AFM, (a-b) images, and (c) corresponding height profile of BNNS-MA.

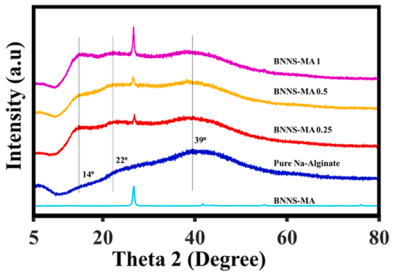

Fig. 2. WAXS pattern of BNNS-MA, Pure Na-Alginate, BNNS-MA 0.25, BNNS-MA 0.5, and BNNS-MA 1.

from the Fig. 2 that the Na-Alginate shows a characteristic broad diffraction peak at 2θ = 14 °, 22 ° and 39 °, which indicates that it is amorphous in nature [33]. BNNS-MA exhibit characteristic peak at 26.8°, similar to bulk BN, which is the main hexagonal plane (002), and it signifies highly crystalline, graphite-like hexagonal structure of BNNS. Additionally, interlayer distance can be calculated with Braggs law, giving distance of 0.33 nm. There are also weaker characteristic peaks at 2θ = 42°, 44°, 55° and 76° that signify 100, 101, 004, and 110 respectively (JCPDS ICSD 34–0421) [33]. In the polymer composite film, these peaks are not appearing due to relatively weaker intensity of these peaks with respect to main peak at 2θ = 26.8°. However, the main hexagonal plane (002) peak is clearly visible at 26.8° even very low concentration of BNNS-MA 0.25 and it indicates that few layers of BNNS-MA has been successfully integrated into the BNNS-MA/Na-Alginate composites. The intensity of this peak at 2θ = 26.8° increases with increase of BNNS-MA concentration (from 0.25 wt% to 1 wt%) and it signifies that presence of higher concentration of few layers of BNNS-MA in BNNS-MA 1 compared to BNNS-MA 0.25 and BNNS-MA 0.5 [34].

4.4. FTIR study

FTIR spectroscopy was performed to identify the interactions between BNNS-MA and Na-Alginate polymer in the fabricated composites and shown in Fig. 3a-b. The FTIR spectrum of Na-Alginate shows clear bands for O-H stretching at 3276 cm^{-1}, C–H stretching of the pyranose ring at 2921 cm^{-1}, carbonyl stretching (C═O) at 1737 cm^{-1}, asymmetric and symmetric C–O stretching of COONa at 1594 cm^{-1} and at 1404 cm^{-1}, C–O–C stretching vibration band at 1021 cm^{-1} respectively. Moreover, the bands at 949 cm^{-1}, 883 cm^{-1} and 814 cm^{-1} correspond to the combined attribute of symmetric stretching of C-O and symmetric stretching C–C–H pyranose ring, symmetric C-O-C stretching of 1,4-glycosidic links, δ C-O-C stretching of guluronic and mannuronic acid respectively [7,32–39]. All the signature peaks for the Na-Alginate are present in FTIR spectra of the nanocomposites but slight shifting is observed in peak position after incorporation of BNNS-MA in Na-Alginate. For example, the stretching vibration for O-H group shifts from 3276 cm^{-1} to 3239 cm^{-1} in BNNS-MA 1. Such kind of displacement to lower wavenumber after incorporation of BNNS-MA correspond to the existence of extensive amount of hydrogen bonding in the composites. As it is reported in previous studies and in FTIR, AFM analyses of the current work that the BNNS-MA sheet consist of high surface area along with few surface functionalities which promotes greater interfacial interactions with Na-Alginate matrix. Higher number of interactions leads to stronger adhesion of the polymeric chains on BNNS-MA surface by intermolecular hydrogen bonding interaction. Most interestingly, the extent of hydrogen bonding interaction increases with the increase of BNNS-MA content which results in the broadening of the peak. Similar kind of effect is also observed in the other reported judicially nano-integrated polymer composite systems [40].

4.5. Thermal property of the composites

To examine thermal stability of BNNS-MA/Na-Alginate composite, TGA studies of BNNS-MA, Pure Na-Alginate, and BNNS-MA/Na-Alginate composite were performed and the obtained TGA thermogram is presented in Fig. 4. It is clear from the Fig. 4 that in the temperature range from 30 to 550 °C, BNNS-MA shows a weight loss of ~1 wt% and this is

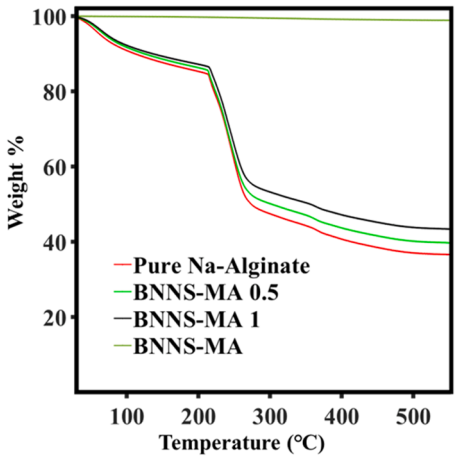

Fig. 4. TGA thermogram of BNNS-MA, pure Na-Alginate film, and BNNS-MA/Na-Alginate composite films.

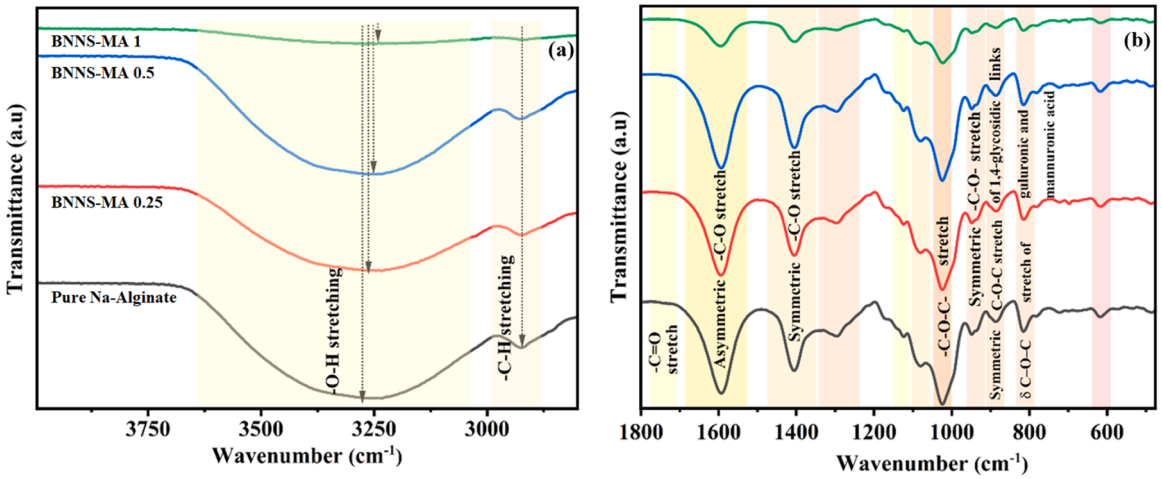

Fig. 3. FTIR spectra of Na-Alginate based composites a) 4000–2500 cm^{-1} b) 1800–500 cm^{-1}.

due to loss of oxygen containing carboxyl acid groups of maleic acid unit of BNNS-MA. It indicates that degree of functionalization of MA is ~1 w % in BNNS-MA [24]. From the thermogram, it can also be seen that Na-Alginate is highly unstable within this temperature range and begins to lose weight at temperatures below 100 ℃. In temperature range 30–100 ℃, the Na-Alginate film shows a weight loss of ~9.1 w% and this is due to the elimination of associated water molecules in the pure Na-Alginate film [35,36,41]. However, it is obvious from the thermogram that BNNS-MA/Na-Alginate composite films exhibit lesser weight loss compared to pure Na-Alginate film and the weight loss is reduced with increase of concentration of BNNS-MA. The BNNS-MA 1 composite shows ~1.4 wt% less weight loss compared to pure Na-Alginate film. It signifies that there is lesser amount of associated water molecules exist in the BNNS-MA/ Na-Alginate composite compared to pure Na-Alginate film. This is due to reduction of availability of H-bonding sites needed for intercalation of water molecules in the BNNS-MA/Na-Alginate composites. From the thermogram, it is also clear that for pure Na-Alginate the onset degradation temperature is ~212 ℃ which increases in correlation with BNNS-MA concentration and reaches ~216 ℃ for BNNS-MA 1 composite film. It indicates that thermal stability of BNNS-MA/Na-Alginate composite films is higher compared to pure Na-Alginate film. In the temperature region of 210–280 ℃, the thermogram of pure Na-Alginate film displays a sharp weight loss of ~35.7 wt%, which is attributed to elimination of functional groups containing oxygen moiety such as hydroxyl and carboxyl acid groups and fragmentation of Na-Alginate molecule [35,36,41]. However, BNNS-MA/ Na-Alginate composite film shows lesser weight loss in this temperature range compared to pure Na-Alginate film. This reduction of weight loss is more intensified with increased of concentration of BNNS-MA, and BNNS-MA 1 composite shows ~5.6 wt% less weight loss compared to pure Na-Alginate film in this temperature range. This is due to strong H-bonding interaction between oxygen containing functional groups of BNNS-MA and Na-Alginate and similar kind of observation in improvement of thermal stability of polymer composites exist in prior art literature [35,36,41]. In the temperature range of 330–550 ℃, the pure Na-Alginate exhibits a weight loss of ~9 w% which is due conversion of fragments and monomeric units to sodium carbonate [35]. In this region, the composite films show lesser weight loss compared to pure Na-Alginate as BNNS-MA 1 composite film exhibits ~6.8 wt% weight loss which is 2.2 wt% less compared to pure Na-Alginate film. It indicates that lesser number of fragments and monomeric units convert to sodium carbonate in the composite films compared to pure Na-Alginate film. This may be due to the homogeneous integration of BNNS-MA into Na-Alginate matrix, which improved the thermal stability of the nanocomposite [42].

4.6. Morphology study

To examine the morphology and dispersion of BNNS-MA in the Na-Alginate matrix, the cross-sectional FESEM studies of pure Na-Alginate and BNNS-MA/Na-Alginate composite films were performed and obtained FESEM images are shown in Fig. 5a-d. FESEM images of the original BN sheets is presented in **ESI** Fig. 1. From the **ESI** Fig. 1 it is clear that h-BN sheets possess a highly aggregated sheets like structure. It is clear from the Fig. 5a, that pure Na-Alginate has continuous polymer matrix where no BNNS-MA was observed. It is also clear from the Fig. 5b-d that BNNS-MA are well-embedded and uniformly dispersed thorough BNNS-MA/Na-Alginate composite films. Additionally, as concentration of BNNS-MA increases, the visibility of dispersed nanosheets increases correspondingly. The dispersed BNNS-MA sheets in Na-Alginate matrixes are marked with white dotted circle in Fig. 5b-d for easier understanding. The AFM study of the BNNS-MA was performed by casting a drop of aqueous dispersion of BNNS-MA from a very dilute solution (0.01 w/v). Hence AFM images and corresponding height profiles indicate that majority of BNNS-MA exhibits highly exfoliated with single and few layer sheets (2–3 layers). However, the composite

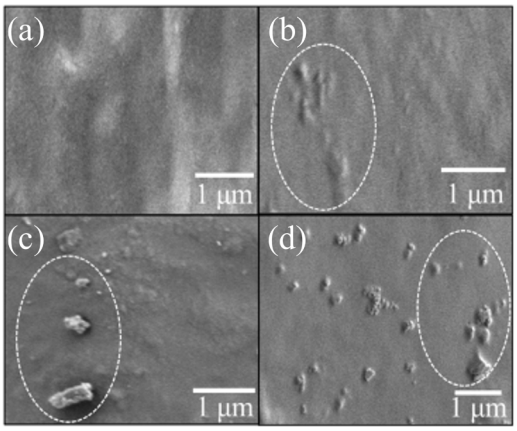

Fig. 5. FESEM images of pure (a) Na-Alginate film and (b-d) BNNS-MA/Na-Alginate composite films.

films for FESEM study were performed at relatively much higher concentration compared to AFM study. As for example BNNS-MA 1 composite was prepared from 0.5 (w/v) aqueous dispersion of BNNS-MA which is 50 times higher concentration compared to aqueous dispersion for AFM study sample (0.01 w/v) and there is possibility of remaining sheet sizes of BNNS-MA with higher thickness. In addition, due to interfacial interaction between BNNS-MA with Na-Alginate, the BNNS-MA sheets surface remain coated with Na-Alginate polymer that can also increase the apparent size of the BNNS-MA sheets in the Na-Alginate composite film. The strong H-bonding interactions between few layers BNNS-MA coated with Na-Alginate and Na-Alginate causes very good compatibilization as well as enhances the dispersion of BNNS-MA in Na-Alginate matrixes. This is also evident from FTIR and TGA results and from similar kind of observations in prior art literature of high-performance nanoparticle integrated polymer composites [43,44]. The scale used for FESEM and AFM images are different. Hence, the appearance of the BNNS-MA sheets is different in AFM and FESEM images, however the enlarged version of the FESEM image of BNNS-MA 1 shown in **ESI** Fig. 2 shows clearly sheets like structure.

4.7. Mechanical property of the composites

To examine mechanical strength and stretchability of BNNS-MA/Na-Alginate composite films, tensile studies of pure Na-Alginate and BNNS-MA/Na-Alginate composites films were performed and resulted stress-strain curves are shown in Fig. 6a. From the stress-strain curve, the stress at break is presented in a bar diagram Fig. 6b. It is obvious from the stress-strain curve and bar diagram that the pure Na-Alginate film exhibits a stress at break of 58 ± 4 MPa with an elongation at break of 9.5 ± 2%. In pure Na-Alginate film, the polymer chains interact with themselves through both inter and intra molecular H-bonding that cause a substantial strength of 58 ± 4 MPa. The elongation at break of 9.5 ± 2% indicates that Na-Alginate films are quite flexible. From the Fig. 6a, it is also clear that the stress at break increases and elongation at break decreases in the BNNS-MA/Na-Alginate composites films compared to Na-Alginate films. The effect of reinforcement of BNNS-MA into the Na-Alginate composites is very prominent, even with very low concentration of BNNS-MA. As for example, in BNNS-MA 0.25 composite film, the stress at break increases from 58 ± 4–70 MPa ± 2.4 MPa whereas elongation of break decreases from 9.5 ± 2% to 8 ± 2.5%. The stress at break increases with increase of BNNS-MA concentration and in composite BNNS-MA 1 it reaches 102 ± 3.5 MPa which is ~73% higher compared to pure Na-Alginate film. However, the elongation at break of the composite films decreases with increase of BNNS-MA concentration and BNNS-MA 1 composite films exhibits an elongation at break of 5.5% which is ~42% lower compared to pure Na-Alginate film. It indicates

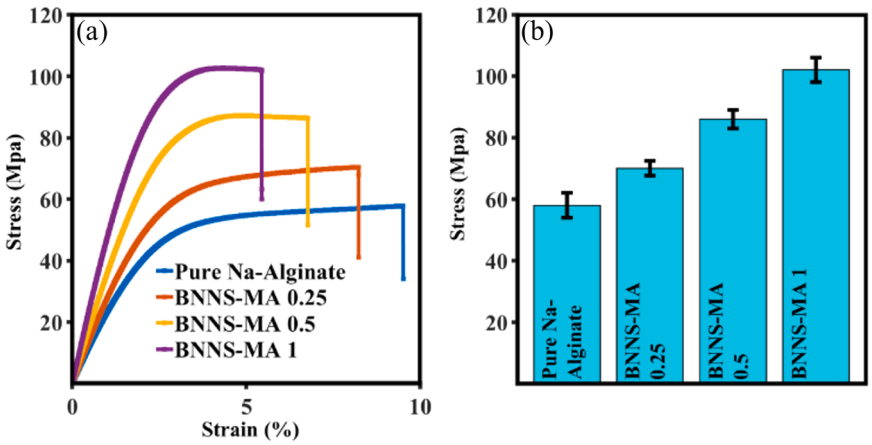

Fig. 6. (a) Stress-strain curve and (b) bar graphs for stress at break for Pure Na-Alginate film and BNNS-MA/Na-Alginate composite films.

that BNNS-MA/Na-Alginate composites films are less ductile compared to pure Na-Alginate composites films. The judicial reinforcement of nanomaterials enhances the mechanical properties of the polymer composite system, and it is the common characteristic of the conventional polymer composites. We conducted a comparative analysis to investigate how functionalizing BNNS with MA impacts its mechanical properties. This analysis involved a comparison between BNNS-MA 1 and BNS 1, and the resulting stress-strain curve can be found in **ESI** Fig. 3. From the **ESI** Fig. 3, it is clear that functionalization of BNNS with MA has significant impact on enhancement of mechanical property of the Na-Alginate composite. The unfunctionalized BNS integrated Na-Alginate composite is more brittle and shows significantly lesser mechanical property compared to MA functionalized BNNS. A few recent reports demonstrated that the homogenous integration and interfacial interaction of functionalized BNNS into polymer matrix plays a vital role to enhance the mechanical characteristics of BNNS/polymer composites [45]. The FESEM image, FTIR spectra, WAXS and TGA results evident that the structure-property relationship of BNNS-MA/Na-Alginate composites is governed by homogeneous distribution of BNNS-MA throughout the Na-Alginate matrix and strong H-bonding interaction between BNNS-MA and Na-Alginate matrix. During tensile testing of the BNNS-MA/Na-Alginate composite films, the Na-Alginate matrix transfers its load to homogeneously dispersed BNNS-MA similarly to other 2-D material polymer composites found in prior art literature [46,47], and this causes a significant amount of improvement in tensile stress of ~73% in BNNS-MA 1 composite compared to pure Na-Alginate film.

4.8. *UV-shielding property of the composite*

To examine UV-blocking properties of BNNS-MA/Na-Alginate composites, UV–vis spectroscopy study of the pure Na-Alginate and BNNS-MA/Na-Alginate composite films with film thickness between ~100 μm was recorded, and the resulted UV–vis spectra are shown in Fig. 7a. We performed a comparative analysis to assess the influence of MA functionalization on the UV-shielding properties of BNNS. This analysis entailed a comparison between BNNS-MA 1 and BNS 1 composite films, with the resulting UV–vis spectra available in **ESI** Fig. 4. It is evident from **ESI** Fig. 4 that the incorporation of 1 wt% of BNNS-MA into a Na-Alginate film significantly enhances its UV-blocking capabilities compared to a BNS 1 composite film. For easier understanding of the UV-blocking properties of the composite films, a bar diagram has been shown in Fig. 7b. Additionally, the digital photographs of pure Na-Alginate and BNNS-MA/Na-Alginate composite films are shown in inset of Fig. 7a to examine visual transparency of the films. It can be observed from Fig. 7a that at wavelengths of 800 nm and 500 nm, the pure Na-Alginate film has transmittance percentages of ~78.4% and ~75.1% respectively. This indicates that pure Na-Alginate film has excellent transparency in visible light region. Furthermore, it can also be observed from Fig. 7a, that pure Na-Alginate exhibits slightly reduced transmittance in UV-regions, with transmittance percentage at wavelengths of 380 nm and 300 nm, which correspond to upper ranges of UVA (315–400 nm) and UVB (280–315 nm) regions, being ~66.5% and ~42.3% respectively. This indicates that Na-Alginate film has some UV-blocking properties that increase with decrease of wavelength. This UV-blocking capability is most likely due to UV-blocking chromophore

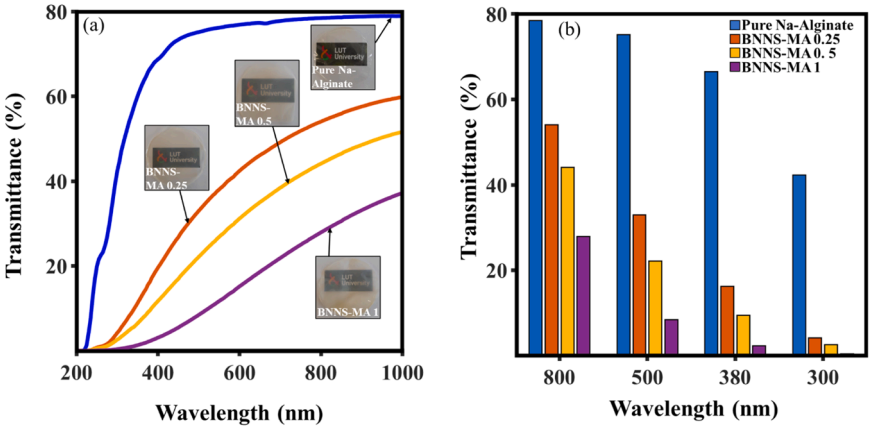

Fig. 7. (a) UV-Vis transmittance spectra with digital photograph at inset and (b) bar diagram of transmittance percentage at specific wavelengths for Pure Na-Alginate film and BNNS-MA/Na-Alginate composite films.

functional groups such as hydroxyl and carboxyl groups present in Na-Alginate [48]. With addition of BNNS-MA into Na-Alginate matrix, it can be observed from Fig. 7(a), that there is a significant reduction in UV-light regions transmittance with very low concentrations of BNNS-MA integration. It can be observed similarly to pure Na-Alginate that in wavelengths of 800 nm and 500 nm, the BNNS-MA 0.25 composite shows a transmittance percentage of ~54.0% and ~33.0% respectively, which is a reduction of ~31.1% and ~56.0% in transmittance percentage in visible light range compared to pure Na-Alginate. Though the visible light transparency decreases with addition of BNNS-MA, the composite film still retains significant amount of transparency, that is also visible in photographs in inset of Fig. 7a. However, the main benefit of BNNS-MA can be seen in UV-regions, where BNNS-MA 0.25 film at wavelengths 380 nm and 300 nm exhibits transmittance percentages of ~16.2% and ~4.2% respectively, which is reduction of ~75.6% and ~90% in transmittance in UVA and UVB regions compared to pure Na-Alginate film. This indicates that even low concentration of BNNS-MA has significant UV-blocking properties, while retaining significant transparency of the composite film. The significant UV-blocking property of BNNS-MA composite is likely due combined effects of the wide band gap of BN in range of ~5.0 – 6.0 eV, which corresponds to wavelength area ~ 200 – 250 nm according to formula $\lambda = \frac{hc}{E_g}$ and chromophore functional groups of Na-Alginate [48, 49]. Additionally, it can be observed from Fig. 7b that a reduction of transmittance in UV-light region increased further with the increased concentration of BNNS-MA in Na-Alginate matrix and BNNS-MA 1 film shows a reduction of transmittance of 99.1% with respect to pure Na-Alginate film at 300 nm.

It is very important to compare the UV-shielding characteristics of our BNNS-MA/Na-Alginate composite films in comparison to previously reported UV-shielding composites to assess the performance of our composite film. For instance, Liu et al. developed a UV-blocking composite using poly(vinyl alcohol) reinforced with 2 wt% of polydopamine-covered zinc oxide particles, achieving around a 96.1% reduction in UV-transmittance while retaining satisfactory transmittance in the visible light region. Their film had a thickness of 55 μm [50]. In another study by Bai et al., an aqueous sodium alginate film was prepared and subsequently crosslinked by coating it with a Fe3 + /EDTA solution containing 27.6 mg/g of ferric ions. This process resulted in a coated film with UV-blocking properties of approximately 98.73% and visible light transmittance of about 65% with a film thickness of around 35 μm [51]. Wang et al. pursued a different approach, dispersing 1.5 wt% of modified TiO2 nanoparticles into a mixture of methyl methacrylate, butyl acrylate, and methacrylic acid through a multi-step process to create a composite film with a thickness ranging from 100 to 200 μm. Their film achieved around 95% UV-light blocking below 350 nm, while maintaining visible region transmittance at about 90% [52]. Our composite film with a thickness of 100 μm shows 95.8% UV-blocking efficiency with only 0.25 wt% of BNNS-MA loading into the Na-Alginate matrix while retaining very good transparency in the visible region which is very significant when comparing with earlier reported literatures.

4.9. Antioxidant and radical scavenging property

To measure the antioxidant behavior of BNNS-MA/Na-Alginate composites, the radical scavenging properties of pure Na-Alginate and BNNS-MA/Na-Alginate composite were measured by 2,2-diphenyl-1-pichydraxyl (DPPH) radical scavenging assay method [53] and resulting UV–vis curve and absorbance bar diagram at wavelength 517 nm are shown in Fig. 8a-b. It can be observed from Fig. 8b that treatment of pure Na-Alginate film with DHHP solution, the reduction in absorbance of DHHP at 517 nm was ~8.8% compared to control sample. This indicates that Na-Alginate has slight radical scavenging properties, which may be due to carbon connected hydrogen scavenging free radicals in the solution [54]. This reduction in absorbance at 517 nm is significantly stronger when DHHP solution is treated with BNNS-MA 1 composite film compared to pure Na-Alginate film and shows ~60.3% decrease in absorbance of DPPH radical compared to control sample. This indicates that addition of BNNS-MA increases the antioxidant properties of Na-Alginate matrix significantly. This is the first study where the antioxidant as well as radical scavenging property of the BNNS-MA has been explored and mechanism of the antioxidant functionalities has been proposed based structural similarity with fullerene, carbon nanotube and graphene [55–57]. DPPH radical scavenging assay results indicates that BNNS-MA has capacity to interact with numerous free radicals and therefore BNNS-MA/Na-Alginate composite film shows better antioxidant property compared to Na-Alginate, even at very low concentration of 1 wt% BNNS-MA integration in the Na-Alginate film. Though, the mechanism of radical scavenging functionality of BNNS-MA has not explored yet, however, it is expected that the BNNS-MA exhibits radical scavenging properties in same fashion as fullerenes, carbon nanotubes, and graphene due to the presence of numerous conjugated double bonds and extremely high electron affinities [55–57]. We undertook a comparative evaluation to assess the influence of MA functionalization on the antioxidant characteristics of BNNS. This examination entailed a direct comparison between BNNS-MA 1 and BNS 1 composite film, and the UV–vis curve derived from the DPPH radical assay method is illustrated in **ESI** Fig. 5. The results from **ESI** Fig. 5 clearly demonstrate that the inclusion of BNNS-MA in a Na-Alginate film notably amplifies its antioxidative potential when compared with a BNS/Na-Alginate film. It is reported that both the BNNS sheets and Na-Alginate have very low

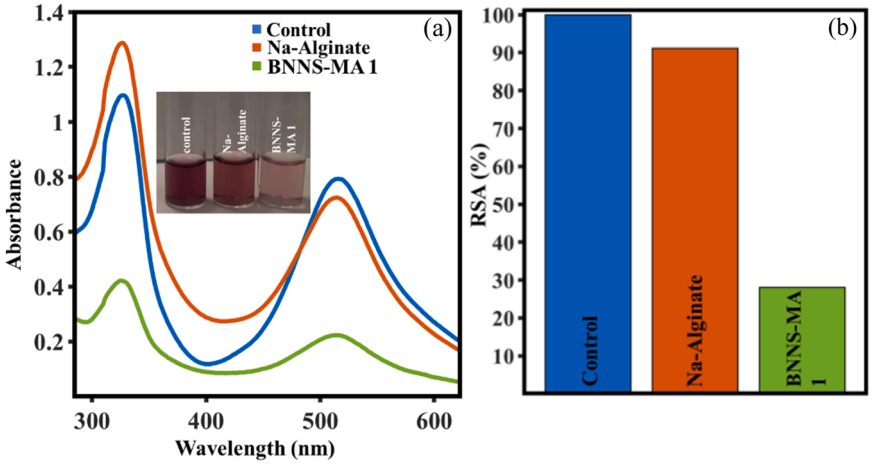

Fig. 8. (a) UV–vis curve and inset digital photograph of DPPH radical assay method and (b) bar diagram of absorbance at wavelength of 517 nm.

cytotoxicity and excellent biocompatibility [7,58]. Therefore, integration of BNNS-MA as an antioxidant in the Na-Alginate film is likely to produce a biocompatible composite film that can improve the shelf life of perishable goods such as medicine, health, beauty, cosmetic and foods.

5. Conclusion

In conclusion, we report fabrication of a high-performance BNNS-MA/Na-Alginate polymer composite with enhanced mechanical, UV-shielding and antioxidation property via integration of low concentrations of BNNS-MA by a simple solution casting method from an aqueous dispersion of BNNS-MA and Na-Alginate solution for first time. The WAXS results confirmed the successful integration of BNNS-MA into Na-Alginate matrix, whereas FTIR results indicate existence of significant interfacial interaction between BNNS-MA and Na-Alginate. The TGA results show slight improvement in thermal stability of the composite film compared to pure Na-Alginate. The cross-sectional FESEM images of the composite films show uniform dispersion of BNNS-MA into Na-Alginate matrix. The UTM results present significant improvement in mechanical strength of BNNS-MA/Na-Alginate polymer composites compared to pure Na-Alginate film, with BNNS-MA 1 composite showing ~73% and ~116% improvement in ultimate stress compared pure Na-Alginate film. The UV–vis spectroscopy measurements also show significant increase in UV-blocking capabilities of BNNS-MA/Na-Alginate composite films while retaining usable amount of visible light transparency with BNNS-MA 1 composite having ~99.1% decrease in transmittance of UV-light at wavelength of 300 nm compared to pure Na-Alginate. BNNS-MA/Na-Alginate composite films shows better antioxidant property compared to pure Na-Alginate. The improved mechanical UV-blocking and antioxidant properties of BNNS-MA/Na-Alginate composite is promising for next generation biobased environmentally friendly cosmetics, consumer and engineering products, and packaging film.

CRediT authorship contribution statement

Timo Elo: Conceptualization, Methodology, Investigation, Validation, Formal analysis, Writing – original draft. **Vijay Singh Parihar**: Investigation, **Abhijit Bera**: Investigation, **Farzin Javanshour**: Writing – review & editing, **Minna Kellomäki**: Writing – review & editing. **Rama Layek**: Investigation, Writing – review & editing, Project administration, Funding acquisition, Supervision.

Declaration of Competing Interest

The authors declare the following financial interests/personal relationships which may be considered as potential competing interests: Rama Layek reports financial support was provided by Kollin säätiö funding for biorefinery programme LUT University, Lahti campus.

Data Availability

Data will be made available on request.

Acknowledgements

Timo Elo acknowledge The Finnish Cultural foundation Päijät-Häme regional fund for providing individual grant for his doctoral study through which this work has conducted. Rama Layek acknowledge Kollin säätiö funding for biorefinery research at LUT University, Lahti campus provided funding for this study. AB acknowledge SERB, India grant under file no. EEQ/2020/000156.

Appendix A. Supporting information

Supplementary data associated with this article can be found in the online version at doi:10.1016/j.colsurfb.2023.113641.

References

[1] R. Geyer, J.R. Jambeck, K.L, Sci. Adv. 3 (7) (2017), e1700782, https://doi.org/10.1126/sciadv.1700782.
[2] A. Sangroniz, J. Zhu, X. Tang, A. Etxeberria, N.X. Chen, H. Sardon, Nat. Commun. 10 (1) (2019), https://doi.org/10.1038/s41467-019-11525-x.
[3] H.T.H. Nguyen, P. Qi, M. Rostagno, A. Feteha, S.A. Miller, J. Mater. Chem. A, Mater. Energy Sustain. 6 (2) (2018) 9298–9331, https://doi.org/10.1039/c8ta00377g.
[4] V. Siracusa, I. Blanco, Polymers 12 (8) (2020) 1641, https://doi.org/10.3390/polym12081641.
[5] J. Chen, A. Wu, M. Yang, Y. Ge, P. Pristijono, J. Li, B. Xu, H. Mi, Food Control 126 (2021), 108063, https://doi.org/10.1016/j.foodcont.2021.108063.
[6] B. Deepa, E. Abraham, N. Cordeiro, M. Mozetic, A.P. Mathew, K. Oksman, M. Faria, S. Thomas, L.A. Pothan, Cellulose 22 (2) (2015) 1075–1090, https://doi.org/10.1007/s10570-015-0554-x.
[7] A. Rhimi, K. Zlaoui, K. Horchani-Naifer, D.J. Ennigrou, Iran. Polym. J. 31 (3) (2022) 367–382, https://doi.org/10.1007/s13726-021-01005-9.
[8] W. Zhang, S. Roy, P. Ezati, D. Yang, J. Rhim, Trends Food Sci. Technol. 136 (2023) 11–23, https://doi.org/10.1016/j.tifs.2023.04.004.
[9] P. Ezati, A. Khan, R. Priyadarshi, T. Bhattacharya, S.K. Tammina, J. Rhim, Food Hydrocoll. 142 (2023), 108771, https://doi.org/10.1016/j.foodhyd.2023.108771.
[10] S. Amrollahi, B. Ramezanzadeh, H. Yari, M. Ramezanzadeh, M. Mahdavian, Compos. Part B Eng. 173 (2019), 106804, https://doi.org/10.1016/j.compositesb.2019.05.015.
[11] D.G. Papageorgiou, I.A. Kinloch, R.J. Young, Prog. Mater. Sci. 90 (2017) 75–127, https://doi.org/10.1016/j.pmatsci.2017.07.004.
[12] M.G. Rasul, A. Kiziltas, B. Arfaei, R. Shahbazian-Yassar, NPJ 2D Mater. Appl. 5 (1) (2021) 1–18, https://doi.org/10.1038/s41699-021-00231-2.
[13] A. Merlo, V.R.S.S. Mokkapati, S. Pandit, I. Mijakovic, Biomater. Sci. 6 (9) (2018) 2298–2311, https://doi.org/10.1039/c8bm00516h.
[14] S. Ghazanfary, F. Oroojalian, R. Yazdian-Robati, M. Dadmehr, A. Sahebkar, Comb. Chem. High. Throughput Screen. 22 (7) (2019) 470–482, https://doi.org/10.2174/1386207322666190930113200.
[15] M. Baysal, K. Bilge, M.M. Yıldızhan, Y. Yorulmaz, Ç. Öncel, M. Papila, Y. Yürüm, Nanoscale; Nanoscale 10 (10) (2018) 4658–4662, https://doi.org/10.1039/c7nr08084k.
[16] X. Jiang, Q. Weng, X. Wang, X. Li, J. Zhang, D. Golberg, Y. Bando, J. Mater. Sci. Technol. 31 (6) (2015) 589–598, https://doi.org/10.1016/j.jmst.2014.12.008.
[17] Y. Huang, Y. Mai, U. Beser, J. Teyssandier, G. Velpula, H. van Gorp, L.A. Straasø, M.R. Hansen, D. Rizzo, C. Casiraghi, R. Yang, G. Zhang, D. Wu, F. Zhang, D. Yan, S. De Feyter, K. Müllen, X. Feng, J. Am. Chem. Soc. 138 (32) (2016) 10136–10139, https://doi.org/10.1021/jacs.6b07061.
[18] C. Du, M. Li, M. Cao, S. Song, S. Feng, X. Li, H. Guo, B. Li, ACS Appl. Mater. Interfaces 10 (40) (2018) 34674–34682, https://doi.org/10.1021/acsami.8b14154.
[19] H. Wu, M.R. Kessler, ACS Appl. Mater. Interfaces 7 (10) (2015) 5915, https://doi.org/10.1021/acsami.5b00147.
[20] V. Yadav, N. Niluroutu, S.D. Bhat, V. Kulshrestha, ACS Appl. Energy Mater. 3 (7) (2020) 7091, https://doi.org/10.1021/acsaem.0c01128.
[21] Z. Wang, Y. Wen, S. Zhao, W. Zhang, Y. Ji, S. Zhang, J. Li, Ind. Crops Prod. 137 (2019) 239–247, https://doi.org/10.1016/j.indcrop.2019.04.054.
[22] W. Cai, B. Wang, L. Liu, X. Zhou, F. Chu, J. Zhan, Y. Hu, Y. Kan, X. Wang, Compos. Part B, Eng. 178 (2019), 107462, https://doi.org/10.1016/j.compositesb.2019.107462.
[23] J. Lee, H. Shin, K.Y. Rhee, Compos. Part B Eng. 157 (2019) 276–282, https://doi.org/10.1016/j.compositesb.2018.08.050.
[24] T. Elo, V. Singh Parihar, R. Nag, A. Bera, R. Layek, Chem. Eng. Sci. 276 (2023), 118820, https://doi.org/10.1016/j.ces.2023.118820.
[25] H. Chand, A. Kumar, P. Bhumla, B.R. Naik, V. Balakrishnan, S. Bhattacharya, V. Krishnan, Adv. Mater. Interfaces 9 (23) (2022), https://doi.org/10.1002/admi.202200508.
[26] M.G. Rasul, A. Kiziltas, B. Arfaei, R. Shahbazian-Yassar, NPJ 2D Mater. Appl. 5 (1) (2021) 1–18, https://doi.org/10.1038/s41699-021-00231-2.
[27] J. Seo, J. Baek, Chemical communications (Cambridge, England), Chem. Commun. 50 (93) (2014) 14651–14653, https://doi.org/10.1039/c4cc07173e.
[28] W. Wang, C. Wang, J. Zheng, F. Shang, J. Dang, X. Zhao, Nanoscale 12 (28) (2020) 15364–15370, https://doi.org/10.1039/d0nr03443f.
[29] S. Sarkar, E. Bekyarova, S. Niyogi, R.C. Haddon, J. Am. Chem. Soc. J. Am. Chem. Soc. 133 (10) (2011) 3324–3327.
[30] K. Kim, A. Hsu, X. Jia, S.M. Kim, Y. Shi, M. Hofmann, D. Nezich, J.F. Rodriguez-Nieva, M. Dresselhaus, T. Palacios, J. Kong, Nano Lett. 12 (1) (2012) 161–166, https://doi.org/10.1021/nl203249a.
[31] V. Vijayaraghavan, L. Zhang, Nanomaterials 8 (7) (2018) 546, https://doi.org/10.3390/nano8070546.
[32] S. Sellimi, I. Younes, H.B. Ayed, H. Maalej, V. Montero, M. Rinaudo, M. Dahia, T. Mechichi, M. Hajji, M. Nasri, Int. J. Biol. Macromol. 72 (2015) 1358–1367, https://doi.org/10.1016/j.ijbiomac.2014.10.016.

[33] F. Guerretta, G. Magnacca, F. Franzoso, P. Ivanchenko, R. Nisticò, Mater. Lett. 234 (2019) 339–342, https://doi.org/10.1016/j.matlet.2018.09.127.
[34] L. Zhai, Z. Liu, C. Li, X. Qu, Q. Zhang, G. Li, X. Zhang, B. Abdel-Magid, 5722-573, RSC Adv. 9 (1) (2019), https://doi.org/10.1039/c8ra10244a.
[35] C.G. Flores-Hernández, Md.L.A. Cornejo-Villegas, A. Moreno-Martell, A. Del Real, Polymers 13 (4) (2021) 504, https://doi.org/10.3390/polym13040504.
[36] F. Ugur Nigiz, Desalination 485 (2020), 114465, https://doi.org/10.1016/j.desal.2020.114465.
[37] D. Şolpan, M. Torun, O. Güven, J. Appl. Polym. Sci. 108 (6) (2008) 3787–3795, https://doi.org/10.1002/app.27945.
[38] M. Yan, J. Shi, S. Tang, L. Liu, H. Zhu, G. Zhou, J. Zeng, H. Zhang, Y. Yu, J. Guo, N. J. Chem. 45 (23) (2021) 1362–1372, https://doi.org/10.1039/d1nj01423d.
[39] M.I. Diana, P.C. Selvin, S. Selvasekarapandian, M.V. Krishna, J. Solid State Electrochem 25 (7) (2021) 2009–2020, https://doi.org/10.1007/s10008-021-04985-z.
[40] R.M. El-Sharkawy, F.S. Abdou, M.A. Gizawy, E.A. Allam, M.E. Mahmoud, Radiat. Phys. Chem. 208 (2023), 110838, https://doi.org/10.1016/j.radphyschem.2023.110838.
[41] M. Ionita, M.A. Pandele, H. Iovu, Carbohydr. Polym. 94 (1) (2013) 339–344, https://doi.org/10.1016/j.carbpol.2013.01.065.
[42] A.A. Bakr, Y.M. Moustafa, M.M.H. Khalil, M.M. Yehia, E.A. Motawea, Can. J. Chem. 93 (3) (2015) 289–296, https://doi.org/10.1139/cjc-2014-0282.
[43] J. Yu, H. Mo, P. Jiang, Polym. Adv. Technol. 26 (5) (2015) 514–520, https://doi.org/10.1002/pat.3481.
[44] R.K. Layek, K.R. Ramakrishnan, E. Sarlin, O. Orell, M. Kanerva, J. Vuorinen, M. Honkanen, J. Mater. Chem. A Mater. Energy Sustain. 6 (27) (2018) 13203–13214, https://doi.org/10.1039/C8TA03651A.
[45] W. Meng, Y. Huang, Y. Fu, Z. Wang, C. Zhi, J. Mater. Chem. C. Mater. Opt. Electron. Devices 2 (47) (2014) 149–161, https://doi.org/10.1039/c4tc01998a.
[46] W. Jiang, C. Sun, Y. Zhang, Z. Xie, J. Zhou, J. Kang, Y. Cao, M. Xiang, Polym. Test. 118 (2023), 107912, https://doi.org/10.1016/j.polymertesting.2022.107912.
[47] G. Go, S. Park, M. Lim, B. Jang, J.Y. Park, H. Cho, Y. Choa, J. Mater. Sci. 57 (38) (2022) 18037–18050, https://doi.org/10.1007/s10853-022-07317-2.
[48] S.R. Derkach, N.G. Voron'ko, N.I. Sokolan, D.S. Kolotova, Y.A. Kuchina, Interactions between gelatin and sodium alginate: UV and FTIR studies, J. Dispers. Sci. Technol. 41 (5) (2020) 690–698, https://doi.org/10.1080/01932691.2019.1611437.
[49] A. Bisht, V. Kumar, P.C. Maity, I. Lahiri, D. Lahiri, Compos. Part B Eng. 176 (2019), 107274, https://doi.org/10.1016/j.compositesb.2019.107274.
[50] H. Liu, W. Liu, D. Hu, W. Ma, B. Deng, Colloids Surf. A Physicochem. Eng. Asp. 648 (2022), 129311, https://doi.org/10.1016/j.colsurfa.2022.129311.
[51] Y. Bai, Y. Zhao, Y. Li, J. Xu, X. Fu, X. Gao, X. Mao, Z. Li, Carbohydr. Polym. 239 (2020), 115480, https://doi.org/10.1016/j.carbpol.2019.115480.
[52] C. Wang, X. Sheng, D. Xie, X. Zhang, H. Zhang, Prog. Org. Coat. 101 (2016) 597–603, https://doi.org/10.1016/j.porgcoat.2016.10.007.
[53] S.B. Kedare, R.P. Singh, J. Food Sci. Technol. 48 (4) (2011) 412–422, https://doi.org/10.1007/s13197-011-0251-1.
[54] M. Falkeborg, L. Cheong, C. Gianfico, K.M. Sztukiel, K. Kristensen, M. Glasius, X. Xu, Z. Guo, Food Chem. 164 (2014) 185–194, https://doi.org/10.1016/j.foodchem.2014.05.053.
[55] M.J. Akhtar, M. Ahamed, H.A. Alhadlaq, A. Alshamsan, Biochim. Et. Biophys. Acta Gen. Subj. 1861 (4) (2017) 802–813, https://doi.org/10.1016/j.bbagen.2017.01.018.
[56] Y. Liu, J. Shi, Nano Today 27 (2019) 146–177, https://doi.org/10.1016/j.nantod.2019.05.008.
[57] Y. Wang, W. Kong, L. Wang, J.Z. Zhang, Y. Li, X. Liu, Y. Li, PCCP, Phys. Chem. Chem. Phys. 21 (3) (2019) 1336–1343, https://doi.org/10.1039/C8CP06768F.
[58] Q. Weng, B. Wang, X. Wang, N. Hanagata, X. Li, D. Liu, X. Wang, X. Jiang, Y. Bando, D. Golberg, ACS Nano ACS Nano 8 (6) (2014) 6123–6130, https://doi.org/10.1021/nn5014808.